Journal of Physics D: Applied Physics

PAPER • **OPEN ACCESS**

Nonheating ozone suppression in pulsed air discharges: role of pulse duration and repetition rate

To cite this article: Sanghoo Park *et al* 2021 *J. Phys. D: Appl. Phys.* **54** 394003

OPEN ACCESS
IOP Publishing
Journal of Physics D: Applied Physics
J. Phys. D: Appl. Phys. **54** (2021) 394003 (8pp)
https://doi.org/10.1088/1361-6463/ac113b

Nonheating ozone suppression in pulsed air discharges: role of pulse duration and repetition rate

Sanghoo Park[1,*], Jinwoo Kim[2], Hyungyu Lee[2], Duksun Han[1], Seungil Park[1], Seong Bong Kim[1] and Wonho Choe[2,3,*]

[1] Institute of Plasma Technology, Korea Institute of Fusion Energy, Gunsan, Republic of Korea
[2] Department of Physics, Korea Advanced Institute of Science and Technology, Daejeon, Republic of Korea
[3] Department of Nuclear and Quantum Engineering, Korea Advanced Institute of Science and Technology, Daejeon, Republic of Korea

E-mail: sanghoopark@kfe.re.kr and wchoe@kaist.ac.kr

Received 28 April 2021, revised 24 June 2021
Accepted for publication 5 July 2021
Published 19 July 2021

Abstract

Facilitating the separate production of ozone (O_3) and nitrogen oxides (NO_x) in air discharges without a thermal process is of most merit in diversifying plasma technology; in particular, it is a primary requirement in certain cold, heat-sensitive plasma applications. Here, we propose a new method of nonheating ozone suppression in air discharges. The present work demonstrates that controlling the plasma chemical kinetics by adjusting the duration (width) and/or repetition frequency of the high-voltage DC pulse is effective in suppressing ozone formation in a surface dielectric barrier discharge in static ambient air. The temporal development of each oxygen- and nitrogen-related species in air discharge is complicated and shows different trends in the time range <10 μs; relatively long-lived O_3 and NO_x are strongly governed by the temporal behavior of short-lived reactive species, such as excited N_2(A) and $N_2(v)$. To quantify time-varying O_3 and NO_x, an *in situ* UV absorption spectroscopy is applied to our gas-tight plasma reactor, which is operated in air at 21 °C. With a fixed frequency at 10 kHz and decreasing pulse duration from 10 μs to 0.18 μs, ozone is quenched faster in the plasma reactor, resulting in an irreversible chemical mode transition from an O_3- to NO-rich environment. From a different set of experiment (with a 200 ns pulse duration and a frequency range of 1–10 kHz), we can conclude that the off-pulse period also plays a crucial role in the temporal evolution of O_3 and NO_x; the larger the applied driving frequency is, the earlier the ozone-free phenomenon appears over the discharge time. Our findings represent a breakthrough in expanding the usage of air discharges and their application in various fields of interest.

Keywords: air discharge, dielectric barrier discharge, nanosecond pulse, plasma chemistry, ozone, nitrogen oxides, ozone-free phenomenon

(Some figures may appear in color only in the online journal)

* Authors to whom any correspondence should be addressed.

1. Introduction

Globally, as part of chemical manufacturing is moving towards 'localization' to meet increasing demands for onsite applications, research areas relevant to decentralizing chemical production are rapidly growing and opening a new era of chemistry and similar fields. Increasing attention has thus been paid to potential technologies, including electrocatalysis [1, 2] and plasma catalysis [3–6]. From a practical standpoint, simple, reliable, and low-maintenance facilities should be primarily considered in conjunction with such chemical production methods. In particular, with the satisfaction of these requirements, since low-temperature plasma has been recognized as 'highly competitive, versatile green technology', various types of plasma sources and technologies have been investigated for application in clinical engineering for nitric oxide (nitric monoxide, NO) production [7, 8] and in chemical engineering for ammonia [3, 9] and hydrogen peroxide [10, 11] synthesis.

Despite many types of plasma apparatus that have been created during the last century, dielectric barrier discharge (DBD) is still considered one of the most scientifically interesting and practically useful plasmas, partly due to its attractive features, such as great operational reliability and reproducibility in atmospheric ambient air. In some of the plasma-aided processes with DBDs developed on a commercial level, the air is mostly or obligatorily used as a background gas instead of pure nitrogen, oxygen, or synthetic dry air because supplying ambient air using conventional compressors is the most cost-effective and simple approaches to improve the running cost-efficiency and maintenance. In such cases, the simultaneous generation of gaseous ozone (O_3) and nitrogen oxide (NO_x) is an unavoidable issue, limiting the practical usage of plasma in certain applications. For example, while ozone is an invaluable species in some plasma applications, from sterilization [12] to gas/water purification [13, 14], ozone-free nitric oxide production is worthy of notice for applications ranging from medical purposes, such as wound disinfection/healing [15, 16] and inhalation therapy [7], to food engineering [17]. Ozone-free plasma operation is particularly imperative for household appliances equipped with a plasma apparatus because exposure to ozone at high concentrations can lead to serious health issues; the maximum ozone level allowed in South Korea is 0.06 ppm in the working environment when exposed for 8 h per day. Thus, facilitating the separate production of ozone and nitrogen oxides in plasma is good for expanding plasma usage and improving its performance for specific purposes, but it is a longstanding challenge in plasma science.

Considering the chemical reactions among O_3 and NO_x ($x = 1$–3), O_3 and NO_3 are major products at room and relatively low temperatures, while NO and NO_2 are dominant at higher temperatures. Thus, most of the NO generators reported thus far are based on arc [18], spark [16], or heated surface [19, 20] discharges, where the gas temperature in such plasma reactors is very high. Malik *et al* [19] reported that in an air-flowing plasma reactor, heating the DBD surface not only eliminated O_3 and minimized NO_2 but also resulted in a significant increase in the concentration and energy yield of the NO product. Park *et al* [20] revealed that the rapid change in the temporal behavior of O_3 and NO_x due to their interplay strongly depended on the reactor temperature, which ranged from 25 °C to 250 °C. In this regard, ongoing efforts have been made to find a way to obtain an ozone-zero mode in plasmas without controlling the gas temperature. Shimizu *et al* [21] and Pavlovich *et al* [22] demonstrated that the time dependence of ozone production in surface DBDs is coupled with the electric power dissipated to the plasma. Both previous studies found that O_3 can be notably suppressed over a certain power density.

As a novel attempt to address the aforementioned issues and practical limitations of air discharges, we here propose a new method of ozone suppression in air discharges without increasing the gas temperature. Control of the temporal chemical kinetics by adjusting the pulse duration and repetition frequency of the high-voltage DC pulse is a key mechanism of this approach. As follows, we are able to demonstrate the ozone-zero phenomenon, free from the gas heating effect by the plasma itself, using a gas-tight chamber equipped with surface DBDs produced in static ambient air, especially and with an *in situ* UV absorption spectroscopy that allowed us to non-invasively and instantaneously measure the time-dependent O_3, NO, and NO_2 concentrations.

2. Methods

Figure 1(a) shows the top and side views of the DBD apparatus, which consisted of two sheet electrodes attached to each side of a 1 mm thick, 100 × 100 mm^2 alumina plate. One electrode was grounded, and the other was connected to a high-voltage DC pulse system consisting of a pulse generator (Directed Energy PVX-4110), a high-voltage DC power supply (Matsusada Precision AU10P-220), and a signal generator (Keysight Technologies 33512B). Both electrodes that are in direct contact with the plasma were composed of a nickel–chromium alloy to prevent rapid oxidation of the electrodes due to highly oxidizing plasma species. Symmetric surface discharges were produced at both sides of the alumina plate, as drawn in figure 1(a), in ambient air (21 °C temperature and 33% relative humidity) using 10 kV unipolar voltage pulses with a driving frequency of 1–10 kHz and a pulse width of 0.18–10 μs. To estimate charge accumulated on the plasma source (not shown here), a 100 nF blocking capacitor was serially connected to the ground electrode. The voltage applied to the DBD source was measured using a 1000:1 high-voltage probe (Tektronix P6015A) connected to a 1 GHz oscilloscope (Tektronix DPO4104B-L), while the voltage across the 100 nF capacitor was measured using a 10:1 voltage probe (Tektronix TPP1000). A current probe (Tektronix P6021A) was used to measure the current waveform.

The DBD plate occupied one of the walls in the test chamber, as illustrated in figure 1(b); thereby only one of the discharge areas was included in the test volume. The surface temperature (T_s) of the DBD apparatus (figure 1(c)) was measured using an infrared (thermal) camera (FLIR A305sc), and the plasma photographs provided in figure 1(d) were taken using

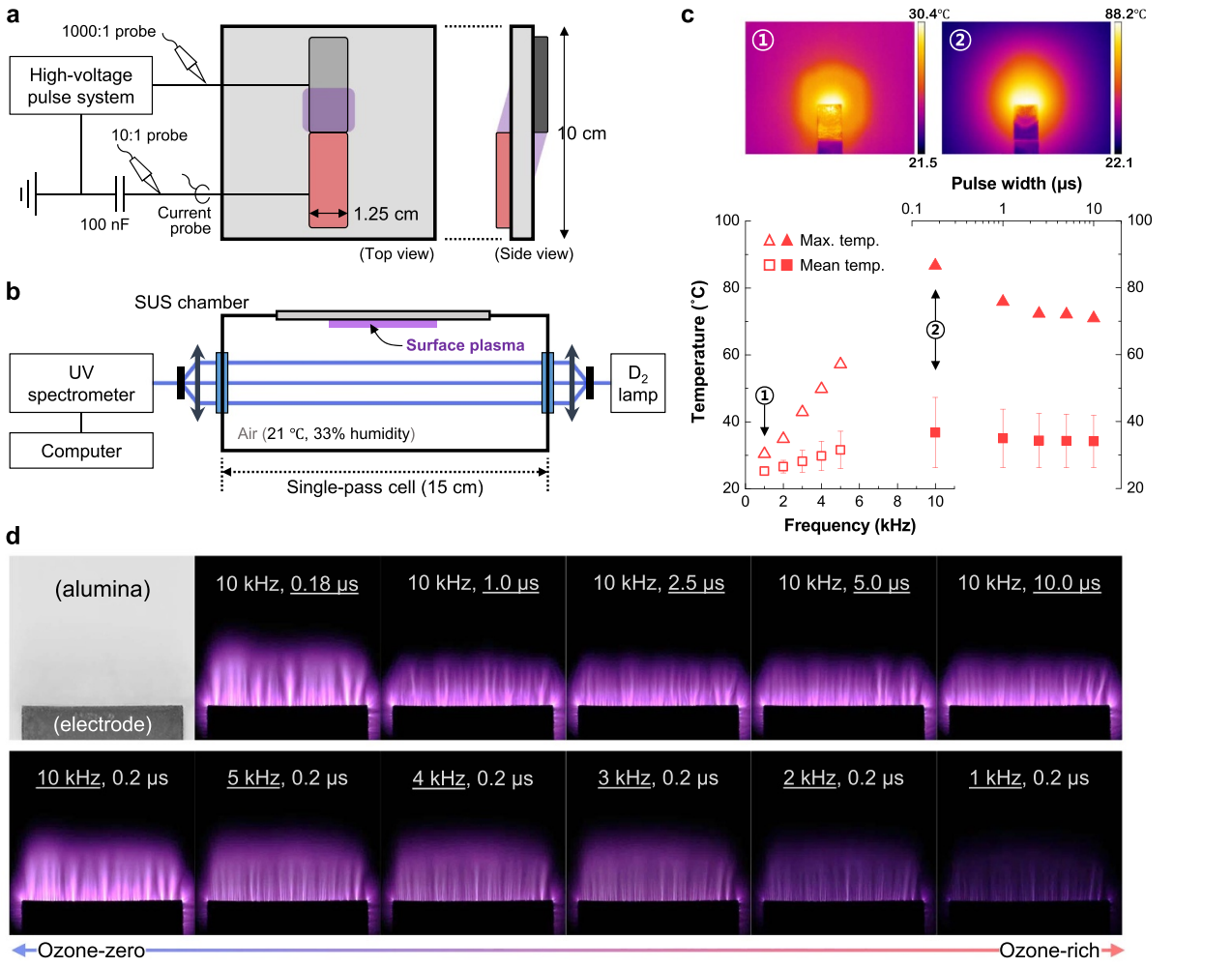

Figure 1. Experimental information on the surface DBD reactor. (a) Schematic drawing (not to scale) of a DBD source configuration consisting of two electrodes and a sandwiched alumina plate with the relevant electronics. (b) Schematics of a plasma chamber equipped with the DBD source and an *in situ* UV absorption spectroscopy system for quantifying ozone- and nitrogen-related species. (c) Two representative infrared (thermal) images, and measured surface temperature of the DBD apparatus as a function of the driving frequency and pulse width for a fixed pulse width of 200 ns (open symbols) and a fixed frequency of 10 kHz (closed). (d) Real photographs of the plasma area and corresponding driving parameters tested in this work. The electrode width of 12.5 mm is used as a substitute for scale bars in (c) and (d).

a Canon EOS 1D Mark II camera combined with a Canon EF 180 mm macro lens. The camera settings of the images were $f/10$, ISO 500, and 0.5 s exposure time. The scattered data in figure 1(c) represent the mean ± SD along with the maximum value in thermal images; two example images are included in the figure. Note that the surface temperature is more essential in the chemical kinetics of the plasma and nearby areas than the gas temperature measured near the surface, for which an underestimated temperature due to the poor thermal conductivity of air can make one overlook thermal deposition of O_3 in similar works.

Instead of the Lissajous method, the time-averaged electric power dissipated to plasma was calculated by multiplying the instantaneous voltage and current traces (figure 2(a)) and then averaging over repetition periods. Note that the different signal delays introduced by the electric probes were taken into account in the process for accurate estimation. The calculated power of plasmas used in this study is presented as a function of the pulse width and repetition frequency in figures 2(b) and (c), respectively.

A cuboid plasma reactor consisting of a gas-tight, stainless-steel chamber (outer dimensions of 15 × 15 × 10 cm^3 and inner volume of 815 cm^3) and two fused silica windows for optical absorption spectroscopy was employed in this work (figure 1(b)). *In situ* UV absorption spectroscopy has merits for this kind of work because O_3, NO, NO_2, and NO_3 can be simultaneously quantified with a good time resolution. Moreover, it is much more cost-effective, easy-to-install, and straightforward than other diagnostics, such as the Fourier transform infrared spectroscopy and laser-based measurements; in particular, it can be nonintrusively applied to plasma reactors without sampling the gas, which induces gas flow and temperature perturbations. The absorption spectra over the wavelength (λ) range of 190–380 nm were obtained using a

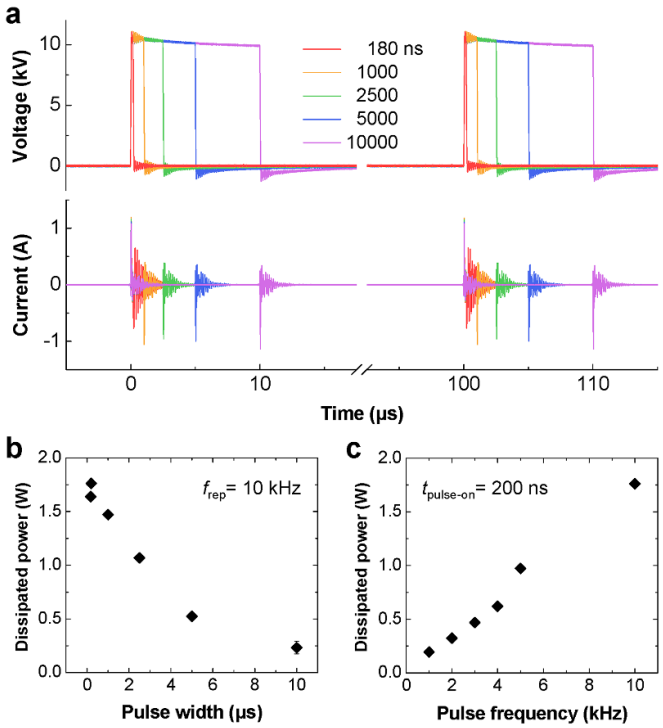

Figure 2. Electrical characteristics of the surface DBD. (a) Voltage and current waveforms with different pulse widths and 10 kHz repetition frequency. (b), (c) Time-averaged power dissipated to the plasma as a function of (b) the pulse width and (c) repetition frequency.

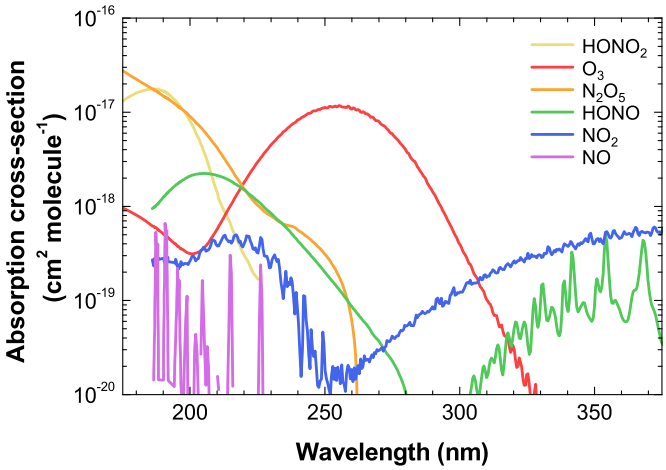

Figure 3. Colored curves showing the spectral absorption cross-sections of chemical species on a log scale in the wavelength range of 175–375 nm: O_3 [23], NO [24], NO_2 [25], N_2O_5 [26], HONO [27], and $HONO_2$ [28].

deuterium (D_2) lamp (Ocean Insight DH-mini) and a spectrometer (Ocean Insight Maya2000 Pro). The absorption path length was set at 150 mm. UV light was guided through an optical fiber (Ocean Insight QP400-2-SR) with a core diameter of 400 μm, and the fiber was connected to a collimating lens adaptor (Ocean Insight 74-UV) to collimate the light into the chamber. The same optical configuration was used to detect the light passing through the chamber volume by the spectrometer, as presented in figure 1(b). The spatial spread of the beam through the lens was 5 mm, and the integration time of spectrometer was 250 ms. Each spectrum used for determining the concentration of each chemical species was obtained by averaging two 250 ms integrated spectra, and therefore the time interval between adjacent data points was 500 ms. All spectra were automatically acquired by a computer.

The absorption cross-section (σ) of ozone and nitrogen-related species over the spectral range of 175–375 nm used in this work is depicted in figure 3. As shown in the figure, each measurable species has its highest cross-section at different wavelengths (e.g. O_3 at 253 nm and NO_2 at 375 nm) or distinctive spectral peaks and profiles (NO, HONO, and $HONO_2$). An extended absorption spectrum in the visible range (not shown here) is sufficient for also quantifying NO_3 in DBD reactors [20]. However, note that estimation of the chemical concentration based on the absorbance at a single selected wavelength, instead of the full spectrum, could lead to an erroneous result. To obtain the synthetic absorption spectra and absolute concentrations of chemical species, the absorbance $A(\lambda)$ was calculated following the Beer–Lambert law, $A(\lambda) = \sum_i n_i l \sigma_i(\lambda)$, where n is the concentration of chemical species in molecules cm^{-3}, l is the absorption path-length (15 cm for this work), and the subscript i indicates each chemical species.

A large amount of nitrous oxide (N_2O) is also produced in air discharges [29]. However, it was not possible to determine its concentration by means of absorption spectroscopy in our case because the absorption cross-section of N_2O at smaller than 220 nm is much lower than that of other species ($HONO_2$ and N_2O_5), and the absorption spectrum of N_2O largely overlaps with the spectra of those species.

Prior to the experiments, repeated cycles of 5 min plasma operation and gas purging were performed several times to avoid an aging effect on the results. Between two successive experiments, plasma-activated air containing O_3 and NO_x from the previous experiment was completely replaced by unpolluted ambient air. After air had filled the chamber, surface DBDs were produced with different voltage waveforms, and UV absorption spectra were simultaneously recorded to quantify chemical species. Each experiment under one driving condition was repeated three times with the same device without any replacements.

3. Results and discussion

Figure 4 shows the time evolution of the absorbance at 253 nm and the corresponding ozone concentration in the DBD reactor with different pulse widths and a fixed repetition frequency (f_{rep}) of 10 kHz. Ozone was actively formed immediately after the plasma was turned on (at $t = 0$ s), and its concentration gradually increased in the first seconds (figure 4(a)). However, the slope of the curves, $dn(O_3)/dt$, that is, the formation rate of O_3, significantly varied with time, depending on the pulse width; the shorter the applied pulse width was, the

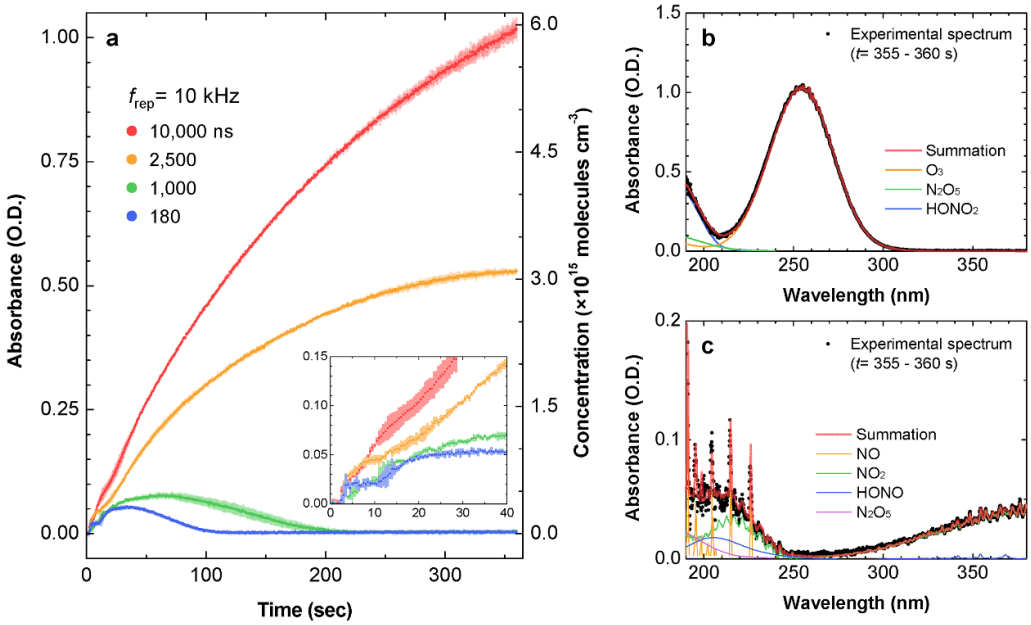

Figure 4. Ozone production in the DBD reactor with different pulse widths. (a) Measured absorbance at a wavelength of 253 nm over the discharge time, indicating the temporal evolution of the ozone concentration. The DBD source was operated with a 10 kHz f_{rep} and a pulse width range of 0.18–10 μs. Data in (a) represent the mean ± SD obtained from three independent measurements. (b), (c) Time-averaged absorption spectra obtained from the (b) 0.18 μs and (c) 10 μs cases at t = 355–360 s, depicted by scatter points. The experimental spectra are compared with fitted synthetic curves obtained from the spectral absorption cross-section of each chemical species given in figure 3. The corresponding concentrations estimated using the nonlinear least squares method are discussed in the text. Plotting the absorbance on a linear scale clearly separates the chemical species.

faster the curve slope decreased (i.e. the faster ozone quenching was). Consequently, in the case of a <1 μs pulse width, the concentration reached a peak at certain times, and the increasing trend was then reversed, which is very similar to the O_3 dynamics in plasma reactors at reactor temperatures greater than 100 °C [20]. Here, neglecting the temperature effects is acceptable since the small variation in the maximum T_s at the DBD surface ($\Delta T_{s,max}$ = 15.7 K) has little to no effect on the O_3 kinetics, as seen in figure 1(c). In addition, the mean T_s was maintained at <40 °C in all investigated cases.

Comparative examples in figures 4(b) and (c) show that the spectral distribution of the time-averaged absorbance in the range of 190–380 nm at t = 355–360 s is sufficient for the identification of chemical species and implies a significant difference in the chemical constituents in the plasma reactor with 0.18 μs and 10 μs pulse widths. In figure 4(b), the fitted synthetic spectrum denoted by a red solid line is a convolution of the spectrum of each species and yields 5.9×10^{15} molecules cm^{-3} of O_3, 4.0×10^{14} molecules cm^{-3} of N_2O_5, and 1.5×10^{15} molecules cm^{-3} of $HONO_2$; these data fit well with the measured spectrum of the 10 μs case. Some species have spectral distributions of absorption cross-sections similar to those of N_2O_5 and $HONO_2$, but these two were chosen in the fitting because the other species have lower concentrations [29] and absorption cross-sections.

Hereinafter, to qualitatively analyze the O_3–NO_x interplay and consequent O_3 dynamics, we referred to the well-simulated chemical kinetics in the DBD afterglow after a single pulse provided in [30] and figure 3 therein. After a single surface discharge is ignited, nitric oxide explosively forms, resulting in a two-order-of-magnitude larger concentration of NO than that of O_3. However, as ozone is logarithmically produced via $O + O_2 + M \rightarrow O_3 + M$ (where M is air molecules), the concentration of NO is rapidly reduced via deep oxidation by O and O_3 (e.g. overall reaction $NO + 2O_3 \rightarrow NO_3 + 2O_2$) and becomes lower than the O_3 concentration at a certain time within a repetition period (100 μs) of the voltage pulse. Consequently, in the larger pulse width cases, O_3 and the products of NO_2 and NO_3 (e.g. via $NO_2 + NO_3 + M \rightarrow N_2O_5 + M$; $2NO_2 + H_2O \rightarrow HONO + HONO_2$; $NO_2 + OH + M \rightarrow HONO_2 + M$) are mainly produced by each single discharge and can be continuously accumulated in the reactor over the discharge time, whereas NO is relatively limited (figures 4(a) and (b)).

On the other hand, in the case of a 180 ns pulse width, NO and NO_2 became the two dominant absorbers while the strong O_3 absorption band entirely disappeared (figure 4(c)); the synthetic spectrum yielded 1.47×10^{15} molecules cm^{-3} of NO, 4.8×10^{15} molecules cm^{-3} of NO_2, 5.33×10^{14} molecules cm^{-3} of HONO, and 1.0×10^{14} molecules cm^{-3} of N_2O_5. The NO_2 concentration gradually increased as the 250–375 nm absorption band appeared, and HONO appearing with NO was observed rather than $HONO_2$ in the absorption spectrum via $NO + OH + M \rightarrow HONO + M$ and $NO + NO_2 + H_2O \rightarrow 2HONO$.

As presented in [30] and figure 3 therein, in the early period of a single discharge (<1 μs), nitric oxide is primarily produced owing to very short-lived species, such as excited $N_2(A)$ and $N_2(v > 4)$, where v is the vibrational

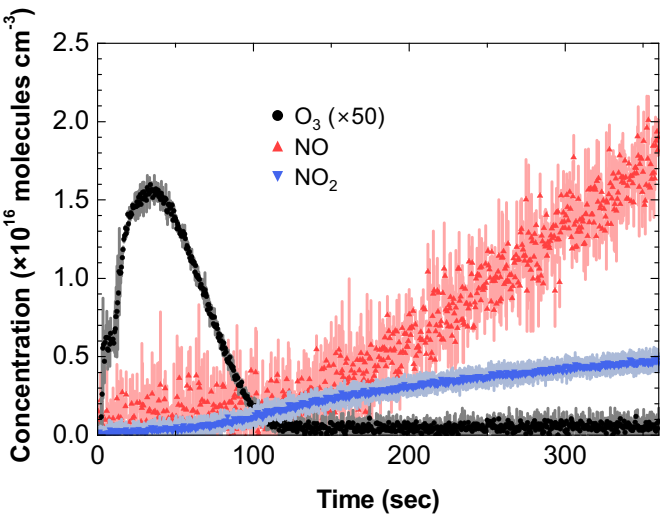

Figure 5. Time evolution of the O_3 (black), NO (red), and NO_2 (blue) concentrations in the plasma reactor operated with a 180 ns pulse width and a 10 kHz f_{rep}. Data are extracted from the absorption spectra, including those in figure 4(c). Note that the ozone concentration is multiplied by 50 for comparison. Data represent the mean ± SD obtained from three independent measurements.

quantum number (e.g. via $O + N_2(A^3\sum) \rightarrow NO + N(^2D)$; $NO_2 + N_2(A^3\sum) \rightarrow NO + O + N_2$; $O + N_2(v) \rightarrow NO + N$), while a small amount of O_3 forms. According to the previous experimental and modeling results in a nanosecond pulse discharge [31] and burst-mode micro discharges [32], the higher the vibrational level v is, the faster the decay of $N_2(v)$ due to the vibrational relaxation of the higher vibrational levels relaxing towards $v = 0$ and 1 levels. This means that the formation rate of NO immediately decreases along with the decay of excited N_2 molecules over the on-pulse time within a repetition period (100 μs) of the voltage pulse. Thus, when a polarity of the surface discharge changes fast before NO and excited N_2 decay by applying a short DC pulse, NO produced by a single discharge can be retained more than O_3, thereby resulting in O and O_3 quenching early, as observed in the 180 ns pulse width case of our experiment. In short, due to the significant difference between NO and O_3 kinetics after a single discharge due to short-lived $N_2(A)$ and $N_2(v)$, we can limit ozone formation in the air discharge by nanosecond pulse operation.

For the sake of direct comparison, the time evolution of the O_3, NO, and NO_2 in the 180 ns case obtained from the absorption spectra is plotted together in figure 5. When the ozone concentration drops and becomes lower than the detection limit within 120 s, both NO and NO_2 steadily accumulate in the reactor. Notably, NO overcomes oxidation reactions and highly exceeds the formation rate and concentration of NO_2, which can be achieved at gas temperatures higher than 300 °C [19].

Along with the chemistry discussed above, transport of the chemical species inside the reactor can also be of great importance. The electrohydrodynamic (EHD) flow, the so-called 'electric wind', induced in weakly-ionized, collisional plasmas (including DBDs) can also play a critical role in the pulse width dependence of O_3 and NO_x. As revealed by our previous work [33, 34], the EHD flow speed decreases and becomes close to zero with decreasing pulse width and fixed f_{rep}. This means that the shorter the pulse width is, the longer the residence time of long-lived species in the plasma region, which is the hottest spot in the reactor (figure 1(c)). We can see peaks and troughs in the curves in the inset of figure 4(a), which implies that chemical transport is clearly affected by the induced electric wind rather than by diffusion. Thus, the ozone formation rate (slope) may be reduced with decreasing pulse width, as seen in the inset. Note that all experiments were conducted in static air; there was no artificial gas flow in the chamber.

Having discussed the role of the on-pulse period (pulse width) in the chemistry in air plasma, we now turn our attention to plasmas with different off-pulse periods. Although the pulse width was fixed at 200 ns, a dramatic change in O_3 production was also observed in cases with a f_{rep} range of 1–10 kHz (figure 6); as f_{rep} was decreased, the maximum O_3 concentration increased, and the decay of O_3 after reaching the peak became slower (figure 6(a)). In particular, the case of 1 kHz f_{rep} showed almost linear $dn(O_3)/dt$, which is considerably different from not only the other cases in figure 6(a) but also the ozone-rich results in figure 4(a). By comparing the absorption spectra in figure 6(b) with those in figures 6(c) and 4(b), nothing was detected other than the O_3 absorption band, indicating that O_3 was exclusively produced in the 1 kHz case. This result implies that DBD with lower pulse frequency and pulse width is capable of producing highly pure O_3.

The time evolution of the O_3 concentration in figure 6(a) is very similar to the result of an earlier study by Shimizu *et al* [21], even though sinusoidal voltage waveforms were used in their experiments. They clearly show the power dependence of the ozone dynamics in a DBD reactor by controlling the frequency in the range of 0.005–10 kHz, corresponding to the input power range of 0.15–2200 mW cm^{-2}, instead of adjusting the voltage amplitude. Nevertheless, the contribution of a raised gas temperature to the thermal decomposition of O_3 with larger input powers has not yet been clarified, and the frequency dependence of the time constant of the $N_2(v)$ vibrational temperature (referred to as τ_v therein) and/or the steady-state vibrational temperature (T^0_{vib}) has remained an open question, and our understanding is as follows.

Because time-resolved populations of $N_2(v)$ exhibit different decay trends—the larger v is, the faster the decay of the $N_2(v)$ population [31]—the long-term variation in $N_2(v)$ populations and the corresponding T_{vib} should be affected by the time interval between two successive pulse discharges. In other words, the time for T_{vib} to reach a sufficient value that determines the $N_2(v > 12)$ population can be decreased with increasing f_{rep}. Moreover, as more pulses are applied in the same period, i.e. a higher f_{rep} is applied, more power is dissipated to the plasma, which leads to more vibrational excitation of $N_2(v)$ and thus a higher T_{vib} [35], which supports the present observation. Comparing figure 6(c) with figure 4(c) partly implies that a sufficiently high T_{vib} is also important to

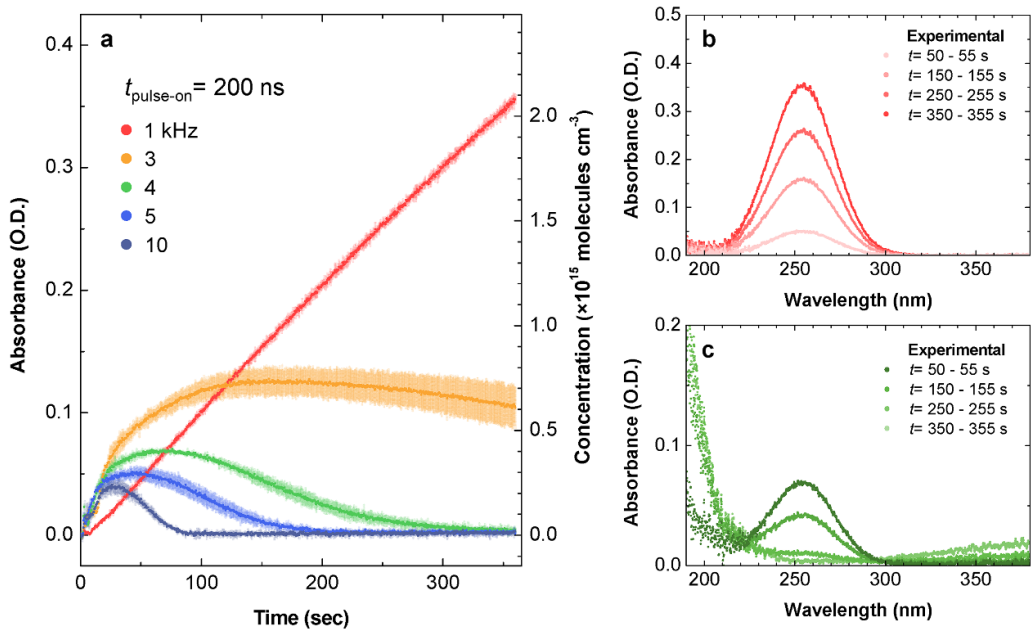

Figure 6. Ozone production in the DBD reactor with different pulse frequencies. (a) Measured absorbance at a wavelength of 253 nm over the discharge time, indicating the temporal evolution of the ozone concentration. The operating condition of the DBD source is a 200 ns pulse width with a f_{rep} range of 1–10 kHz. Data in (a) represent the mean ± SD obtained from three independent measurements. (b), (c) Time-dependent absorption spectra obtained from the (b) 1 kHz and (c) 4 kHz f_{rep} cases.

produce a NO-rich mode; otherwise, NO_2 and $HONO_2$ instead become dominant after O_3 quenching.

One possible scenario of abundant O_3 with regard to the 1 kHz case is as follows. The reduced gap voltage of the 1 kHz pulsed DBD due to the long off-pulse period can lead to operation with diffusive surface discharges (called silent discharges) in the absence of filament discharges (see figure 1(d)), which show higher electron energy and ro-vibrational temperatures of N_2. This means that such mild operation of DBD with a lower f_{rep} can minimize O_3 quenching and create O_3-enriched conditions.

4. Conclusion

In our experiments, ozone-zero plasma operation is successfully achieved with sub-microsecond pulse widths and sufficiently high frequencies, although the spatially averaged surface temperature of the DBD apparatus is maintained at <40 °C, which is naturally raised by the plasma itself. In most cases, in the early discharge phase, O_3 formed rapidly and an O_3-dominant environment was created in the plasma reactor. After a certain time, depending on the pulse width and frequency, the absorption spectrum showed a continuous increase in NO and NO_2 over time, whereas the O_3 level was reasonably diminished, which is called the chemical mode transition from O_3 to NO_x or the O_3-zero phenomenon. This mode transition and the consequent ozone-zero phenomenon occur faster over the plasma-on time with decreasing pulse width and increasing frequency. Our findings indicate that tailoring $N_2(A)$ and $N_2(v)$ by adjusting the pulse width or tailoring T_{vib} by adjusting the pulse frequency is a breakthrough approach in air plasma chemistry. We believe that understanding the nonlinear effect of the duration and repetition rate of DC pulses on long-term O_3 and NO_x dynamics will lead to better control and optimization of air discharges, especially for applications in biomedical, food, and agriculture industries.

Author contributions

S Park and W C conceived of the experiments. S Park and J K conducted all experiments. S P have prepared the manuscript and figures, and all authors have participated in the improvement of the paper.

Data availability statement

The data that support the findings of this study are available upon reasonable request from the authors.

Acknowledgments

This work was supported by the R&D Program of 'Plasma Advanced Technology for Agriculture and Food (No. 1711124797)' through the Korea Institute of Fusion Energy (KFE) funded by the Government funds, Republic of Korea. This work was also supported by the National Research Foundation of Korea (NRF) grant funded by the Korea government (No. 2020R1C1C1004645).

ORCID iDs

Sanghoo Park https://orcid.org/0000-0002-4180-7455
Wonho Choe https://orcid.org/0000-0002-8952-8252

References

[1] Zhang J, Zhang H, Cheng M-J and Lu Q 2020 Tailoring the electrochemical production of H_2O_2: strategies for the rational design of high-performance electrocatalysts *Small* **16** 1902845

[2] Singh N and Goldsmith B R 2020 Role of electrocatalysis in the remediation of water pollutants *ACS Catal.* **10** 3365–71

[3] Mehta P, Barboun P, Herrera F A, Kim J, Rumbach P, Go D B, Hicks J C and Schneider W F 2018 Overcoming ammonia synthesis scaling relations with plasma-enabled catalysis *Nat. Catal.* **1** 269–75

[4] Bogaerts A *et al* 2020 The 2020 plasma catalysis roadmap *J. Phys. D: Appl. Phys.* **53** 443001

[5] Hong J, Prawer S and Murphy A B 2018 Plasma catalysis as an alternative route for ammonia production: status, mechanisms, and prospects for progress *ACS Sustain. Chem. Eng.* **6** 15–31

[6] Shah J, Wang W, Bogaerts A and Carreon M L 2018 Ammonia synthesis by radio frequency plasma catalysis: revealing the underlying mechanisms *ACS Appl. Energy Mater.* **1** 4824–39

[7] Yu B, Muenster S, Blaesi A H, Bloch D B and Zapol W M 2015 Producing nitric oxide by pulsed electrical discharge in air for portable inhalation therapy *Sci. Trans. Med.* **7** 294ra107

[8] Kühn S, Bibinov N, Gesche R and Awakowicz P 2010 Non-thermal atmospheric pressure HF plasma sources: generation of nitric oxide and ozone for bio-medical applications *Plasma Sources Sci. Technol.* **19** 015013

[9] Hawtof R, Ghosh S, Guarr E, Xu C, Sankaran R M and Renner J N 2019 Catalyst-free, highly selective synthesis of ammonia from nitrogen and water by a plasma electrolytic system *Sci. Adv.* **5** eaat5778

[10] Liu J, He B, Chen Q, Li J, Xiong Q, Yue G, Zhang X, Yang S, Liu H and Liu Q H 2016 Direct synthesis of hydrogen peroxide from plasma-water interactions *Sci. Rep.* **6** 38454

[11] Chen Z, Liu D, Chen C, Xu D, Liu Z, Xia W, Rong M and Kong M G 2018 Analysis of the production mechanism of H_2O_2 in water treated by helium DC plasma jets *J. Phys. D: Appl. Phys.* **51** 325201

[12] Park J Y, Park S, Choe W, Yong H I, Jo C and Kim K 2017 Plasma-functionalized solution: a potent antimicrobial agent for biomedical applications from antibacterial therapeutics to biomaterial surface engineering *ACS Appl. Mater. Interfaces* **9** 43470–7

[13] Foster J E 2017 Plasma-based water purification: challenges and prospects for the future *Phys. Plasmas* **24** 055501

[14] Malik M A 2010 Water purification by plasmas: which reactors are most energy efficient? *Plasma Chem. Plasma Process.* **30** 21–31

[15] Butenko A V, Shekhter A B, Pekshev A V, Vagapov A B, Fayzullin A L, Serejnikova N B, Sharapov N A, Zaborova V A and Vasilets V N 2020 Review of clinical applications of nitric oxide-containing air-plasmas gas flow generated by Plason device *Clin. Plasma Med.* **19–20** 100112

[16] Dobrynin D, Arjunan K, Fridman A, Friedman G and Clyne A M 2011 Direct and controllable nitric oxide delivery into biological media and living cells by a pin-to-hole spark discharge (PHD) plasma *J. Phys. D: Appl. Phys.* **44** 075201

[17] Jung S, Kim H J, Park S, Yong H I, Choe J H, Jeon H-J, Choe W and Jo C 2015 The use of atmospheric pressure plasma-treated water as a source of nitrite for emulsion-type sausage *Meat Sci.* **108** 132–7

[18] Qian L, Wenlu Z, Hong W, Juan D, Xinli T, Linlin W and Hong S 2020 Design and study of nitric oxide portable producing device using continuous discharging arc plasma reaction keeping low energy efficiency for viral pneumonia emergency therapy *PLoS One* **15** e0237604

[19] Malik M A, Jiang C, Heller R, Lane J, Hughes D and Schoenbach K H 2016 Ozone-free nitric oxide production using an atmospheric pressure surface discharge—a way to minimize nitrogen dioxide co-production *Chem. Eng. J.* **283** 631–8

[20] Park S, Choe W and Jo C 2018 Interplay among ozone and nitrogen oxides in air plasmas: rapid change in plasma chemistry *Chem. Eng. J.* **352** 1014–21

[21] Shimizu T, Sakiyama Y, Graves D B, Zimmermann J L and Morfill G E 2012 The dynamics of ozone generation and mode transition in air surface micro-discharge plasma at atmospheric pressure *New J. Phys.* **14** 103028

[22] Pavlovich M J, Clark D S and Graves D B 2014 Quantification of air plasma chemistry for surface disinfection *Plasma Sources Sci. Technol.* **23** 065036

[23] Molina L T and Molina M J 1986 Absolute absorption cross sections of ozone in the 185 to 350 nm wavelength range *J. Geophys. Res.* **91** 14501–8

[24] Thompson B A, Harteck P and Reeves R R Jr 1963 Ultraviolet absorption coefficients of CO_2, CO, H_2O, N_2O, NH_3, NO, SO_2, and CH_4 between 1850 and 4000 Å *J. Geophys. Res.* **68** 6431–6

[25] Bass A M, Ledford A E and Laufer A H 1976 Extinction coefficients of NO_2 and N_2O_4 *J. Res. Natl Bur. Stand.* **80A** 143–66

[26] Osborne B A, Marston G, Kaminski L, Jones N C, Gingell J M, Mason N, Walker I C, Delwiche J and Hubin-Franskin M-J 2000 Vacuum ultraviolet spectrum of dinitrogen pentoxide *J. Quant. Spectrosc. Radiat. Transfer* **64** 67–74

[27] Sander S P *et al* 2011 *Chemical Kinetics and Photochemical Data for Use in Atmospheric Studies, Evaluation Number 17, JPL Publication 10–6* (Jet Propulsion Laboratory) (available at: http://jpldataeval.jpl.nasa.gov/) (Accessed 10 June 2011)

[28] Suto M and Lee L C 1984 Photoabsorption and photodissociation of $HONO_2$ in the 105–220 nm region *J. Chem. Phys.* **81** 1294–7

[29] Sakiyama Y, Graves D B, Chang H-W, Shimizu T and Morfill G E 2012 Plasma chemistrymodel of surface microdischarge in humid air and dynamics of reactive neutral species *J. Phys. D: Appl. Phys.* **45** 425201

[30] Baldus S, Schröder D, Bibinov N, von der Gathen V S and Awakowicz P 2015 Atomic oxygen dynamics in an air dielectric barrier discharge: a combined diagnostic and modeling approach *J. Phys. D: Appl. Phys.* **48** 275203

[31] Shkurenkov I, Burnette D, Lempert W R and Adamovich I V 2014 Kinetics of excited states and radicals in a nanosecond pulse discharge and afterglow in nitrogen and air *Plasma Sources Sci. Technol.* **23** 065003

[32] Šimek M, Ambrico P F and Prukner V 2015 LIF study of $N_2(A^3\Sigma_u^+, v = 0–10)$ vibrational kinetics under nitrogen streamer conditions *J. Phys. D: Appl. Phys.* **48** 265202

[33] Park S, Cvelbar U, Choe W and Moon S Y 2018 The creation of electric wind due to the electrohydrodynamic force *Nat. Commun.* **9** 371

[34] Park S, Choe W, Lee H, Park J Y, Kim J, Moon S Y and Cvelbar U 2021 Stabilization of liquid instabilities with ionized gas jets *Nature* **592** 49–53

[35] van Alphen S, Vermeiren V, Butterworth T, van den Bekerom D C M, van Rooij G J and Bogaerts A 2020 Power pulsing to maximize vibrational excitation efficiency in N_2 microwave plasma: a combined experimental and computational study *J. Phys. Chem.* C **124** 1765–79